Auxin-dependent xyloglucan remodelling defines differential tissue expansion in *Arabidopsis thaliana*

Silvia Melina Velasquez[1], Marçal Gallemi[2,§], Bibek Aryal[3,§], Peter Venhuizen[1], Elke Barbez[1], Kai Dünser[1], Maria Kalyna[1], Grégory Mouille[4], Eva Benkova[2], Rishikesh Bhalerao[3] and Jürgen Kleine-Vehn[1,*]

[1] Department of Applied Genetics and Cell Biology, University of Natural Resources and Life Sciences Vienna (BOKU), Muthgasse 18, 1190 Vienna, Austria.

[2] Institute of Science and Technology Austria, Klosterneuburg, 3400, Austria.

[3] Department of Forest Genetics and Plant Physiology, Umeå Plant Science Centre, Swedish University of Agricultural Sciences, SE-901 87 Umeå, Sweden.

[4] Institut Jean-Pierre Bourgin, Institut National de la Recherche Agronomique, AgroParisTech, CNRS, Université Paris-Saclay, 78000 Versailles, France.

[§] Equal contributions

*Correspondence and requests for materials should be addressed to J.K.-V. (juergen.kleine-vehn@boku.ac.at)

Size control is a fundamental question in biology, showing incremental complexity in case of cell wall surrounded plant cells. Here we show that auxin signalling restricts the complexity of extracellular xyloglucans, which defines cell wall properties and tissue expansion. Our work uncovers an alternative mechanism of how the phytohormone auxin modulates the cell wall for steering differential growth control in gravitropic hypocotyls.

The phytohormone auxin has outstanding importance for plant growth and development. Despite its significance, we just start to understand the subcellular mechanisms by which auxin exerts growth control of a cell wall-encapsulated plant cell. In a concentration- and cell-type-dependent manner, auxin signalling steers promotion and repression of cell expansion (Sauer et al., 2013). These cellular levels of auxin rely on a complex interplay between its metabolism and intercellular transport (Rosquete et al., 2012; Sauer and Kleine-Vehn, 2019). On the other hand, tissue specific expression of auxin signalling components

and intracellular auxin transport define the cellular sensitivity to auxins (Barbez et al., 2012; Béziat et al., 2017; Calderón Villalobos et al., 2012). Canonical auxin responses take place in the nucleus via auxin binding to its co-receptors TIR1/AFBs and transcriptional repressor Aux/IAAs (Lavy and Estelle, 2016). Auxin-dependent control of cellular expansion is in part manifested by stiffening or loosening of the cell wall (Majda and Robert, 2018), but the underlying molecular mechanisms remain long-standing research questions. The plant cell wall is a complex, composite structure comprised mainly of polysaccharides, such as cellulose microfibrils, hemicellulose (including branched xyloglucans and arabinoxylans), a diverse pectin matrix and proteoglycans (including extensins and arabinogalactan proteins) (Cosgrove, 2005). The acid growth theory proposes that auxin-dependent increased activity of the plasma membrane proton pump triggers rapid cell wall acidification. The decrease of extracellular pH initiates a cascade of events, including the activation of expansins, which dissociate xyloglucan-cellulose networks and consequently promote cell wall loosening (Cosgrove, 2014; Dünser and Kleine-Vehn, 2015). However, the complex concentration- and tissue-dependent effects of auxin questions the universal validity of this acid growth theory [e.g. (Barbez et al., 2017; Calderón Villalobos et al., 2012; Pacheco-Villalobos et al., 2016)]

In order to identify additional/alternative mechanisms that may define cellular sensitivity to auxin in the cell wall, we made use of dark grown hypocotyls of *Arabidopsis thaliana*. This structure is not only an excellent model for cell expansion, but in addition, unlike roots, requires genomic responses to execute auxin-dependent growth control (Fendrych et al., 2018; Fendrych et al., 2016). In order to identify *bona fide* auxin-regulated genes in this context, we endogenously decreased and increased auxin levels in dark grown hypocotyls, using estradiol-inducible auxin-conjugating enzyme GH3.6 (Staswick et al., 2005) and auxin-biosynthesis enzyme YUC6 (Cheng et al., 2006). Compared to the empty vector control, 1909 and 2177 genes were differentially expressed after a three hours induction of GH3.6 and YUC6, respectively (STable1). The overlapping genes clustered in four categories, displaying (I) up- or (II) down-regulation in both as well as (III) up- and down- or (IV) down- and up- in YUC6 and GH3.6 induced dark grown hypocotyls, respectively (Fig.1A-B; STable1). In total we identified 102 genes, which showed inverse (category III and IV) regulation in high and low auxin conditions. On the other hand, 133 and 230 overlapping genes (category I and II) showed up and down regulation in response to any alteration in auxin levels,

respectively (Fig.1A-B; STable1). This set of data suggests a complex and partially overlapping genomic read out of low and high auxin conditions.

Among the differentially expressed genes (STable1), which we assume to be *bona fide* auxin regulated genes in dark grown hypocotyls, the GO-term analysis showed enrichment for auxin- and cell wall-related pathways (STable2). Within the full list of differentially expressed genes (DEG) in both YUC6 and GH3.6, cell wall modifying genes of the *Xyloglucan endotransglucosylase/ hydrolase* (*XTH*) family were particularly prominent (SFig.1, SFig.2, STable1). Xyloglucan (XyG) is an extracellular β-1,4 glucose polymer with functional glycosyl side-chains. In *Arabidopsis thaliana*, 75% of the glucose residues are substituted with a xylosyl residue, which can be further substituted (20-30%) with galactose. Finally, the galactose moiety can be decorated with a fucose or an *O-acetyl* group (overview in SFig.1) (Cosgrove, 2005; Schultink et al., 2014). *XTHs* can catalyse XyG endotransglucosylase activity (XET) by cleaving and selectively re-joining XyG molecules in the apoplast, which could locally weaken the cell wall and allow for cell expansion (Cavalier et al., 2008; Farkas et al., 1992; Franková and Fry, 2013; Fry et al., 1992b; Nishitani and Tominaga, 1992). Notably, XyG structure itself affects the substrate recognition of the *XTHs*, providing additional complexity to its regulation (Fry et al., 1992a; Fry, 1997; Lorences and Fry, 1993; Vissenberg et al., 2000). Several studies have proposed a potential link between genomic auxin responses and XyG related genes (Catalá et al., 1997; Catalá et al., 2001; Osato et al., 2006; Sánchez et al., 2003; Talbott and Ray, 1992; Vissenberg et al., 2005; Xu et al., 1995; York et al., 1984), but the functional importance of such an interplay remains unknown.

YUC6 induction increased the expression of several *XTH* genes, whereas *GH3.6* expression had a comparatively weaker impact (SFig.2). Similarly, kynurenin-induced, pharmacological inhibition of auxin biosynthesis (He et al., 2011) and PIN-like (PILS) intracellular auxin transport-induced repression of nuclear auxin signalling (Barbez et al., 2012; Béziat et al., 2017; Feraru et al., 2019) exerted a weak effect on *XTH* genes (Fig.1C). Accordingly, most *XTH* genes seem primarily responsive to increased auxin levels. To assess if XyGs may contribute to auxin-reliant processes, we initially assessed whether genetic interference with *XTH* function, such as auxin inducible cluster of *XTH30* and *XTH33* (SFig.2), may impact on auxin-sensitive growth. Notably, the hypocotyl growth of *xth30* and *xth33* knock-out mutants displayed hypersensitivity to auxin (Fig.2A-B). To further study this

interaction, we partially reduced nuclear auxin signalling in *xth33* mutant by crossing a *PILS5* overexpressor (PILS5^{OE}) into the *xth33-1* mutant background. Compared to the parental lines, PILS5^{OE} in *xth33* mutant background alleviated the growth reduction in dark grown hypocotyls (Fig.2C-D; SFig.3A), proposing an interdependency of nuclear auxin signalling and XyG remodelling during hypocotyl expansion.

Besides the transcriptional effects (SFig.2), also the XyG structure itself could contribute to *XTH* activity (Fry et al., 1992a; Fry, 1997; Lorences and Fry, 1993; Vissenberg et al., 2000). Hence, we assessed if PILS5-induced repression of nuclear auxin signalling correlates with changes in wall composition. PILS5 induction induced moderate alterations in extracellular monosaccharides, showing slightly increased galactose as well as mildly decreased levels of rhamnose and xylose in dark grown hypocotyls (SFig.4). To further depict the XyG structure, we used oligosaccharide mass profiling (OLIMP) (Lerouxel et al., 2002) and most prominently observed an increase in fucosylation of XyGs in *PILS5* overexpressing lines (Fig.2E).

Our data suggests that PILS-dependent repression of nuclear auxin signalling favours complex XyGs structures. To further investigate the effect of endogenous auxin levels on the composition of XyGs, we induced asymmetric tissue distribution of auxin by gravi-stimulating dark grown hypocotyls (Rakusová et al., 2011). We used the specific CCRC-M1 antibody, which detects fully complex, fucosylated XyG-epitopes (Puhlmann et al., 1994) and thereby allowed us to monitor spatial alterations in XyG complexity. We observed a gravity induced asymmetry of CCRC-M1 labelling (Fig.2F-G), revealing that asymmetric auxin accumulation correlates with altered XyG composition in dark grown hypocotyls.

Based on these independent approaches, we assume that auxin impacts on the structure of XyGs. Notably, the galactosyltransferase *MUR3,* but not the galactosidase *bGAL10* (Jensen et al., 2012; Madson et al., 2003; Sampedro et al., 2012) was reproducibly up-regulated after *YUC6* induction (SFig.5A-B). On the other hand, the transcription of fucosyltransferase *MUR2* and the fucosylhydrolase *AXY8/FUC95A* (Günl et al., 2011; Reiter et al., 1997; Vanzin et al., 2002) were not markedly altered (SFig.5A-B). Hence, to initially address whether fucosylation and/or galactosylation status of XyGs defines cellular sensitivity to auxin, we exposed the *mur2* and *axy8* as well as *mur3* and *bgal10* dark grown mutants to auxin (IAA 800nM). Under these conditions, auxin-sensitive hypocotyl growth rate (length) of the XyG mutants was largely not distinguishable from wild type (Fig.3A-F;

SFig.6A-C), but particularly *mur3-3* mutants displayed an exacerbated loss of gravitropic growth (Fig.3A-D). The curved *mur3* mutant dark grown hypocotyl phenotype was reminiscent to wild type seedlings exposed to high levels of exogenous auxin (Fig.3E-F), possibly indicating hypersensitivity of *mur3* mutants to auxin. In agreement with hypersensitive auxin responses, *mur3* mutant hypocotyls showed gravitropic hyper-bending responses when challenged with a 90° angle change in growth orientation (Fig.4A-C). Conversely, *bgal10-1* showed slower gravitropic growth kinetics when compared to wild type (Fig.4D), which agrees with its partially auxin resistant hypocotyl growth (Fig.3E-F).

Overall, this set of data pinpoint to the importance of XyGs for cellular sensitivity to auxin. XyGs contribute to tissue mechanics (Zhao et al., 2019) and its galactose residue seems particularly important for the mechanical strength of primary cell walls (Peña et al., 2004) This raises the question whether *MUR3*-dependent galactosylation of XyG could be implicated in auxin-dependent modulation of cell wall properties. To assess such a potential link, we next performed atomic force microscopy (AFM) and analysed the contribution of *MUR3* to cell wall mechanics. Notably, the cell walls of untreated dark grown *mur3-3* mutant hypocotyls were much stiffer when compared to wild type (Fig.4E-F), correlating with an overall reduction in hypocotyl growth (SFig.6A). On the other hand, exogenously applied auxin (IAA, 800nM) induced stronger loosening of *mur3* mutant cell walls when compared to wild type (Fig.4E-F), which could explain the enhanced differential growth response in gravitropic dark grown hypocotyls. This finding suggests that *MUR3* defines the auxin effect on cell wall mechanics in dark grown hypocotyls.

In conclusion, our data shows that genomic auxin responses modulate XyG related genes, including *XTH30, XTH33,* and *MUR3*, which contribute to auxin sensitivity. In agreement, auxin induces alterations in XyG composition and defines cell wall mechanics in a XyG-reliant manner. Our set of data uncovers a developmentally important role for XyGs in setting auxin-dependent growth control in gravitropic dark grown hypocotyls. Accordingly, we propose an alternative, XyG-dependent mechanism to be operational in auxin-reliant growth control in the extracellular space. It remains to be investigated if this mechanism is also linked to (possibly *XTH*-reliant) specific cleavage and release of XyG moieties, because fucosylated XyG oligosaccharides could provide a negative feedback on auxin responses (McDougall and Fry, 1989; York et al., 1984).

Acknowledgements

We are grateful to Paul Knox, Markus Pauly, Malcom O'Neill, and Ignacio Zarra for providing published material; the BOKU-VIBT Imaging Center for access and M. Debreczeny for expertise; the Vienna BioCenter Core Facility for sequencing; Georg Seifert and Jozef Mravec for critical reading. This work was supported by the Vienna Science and Technology Fund (WWTF) (to J.K.-V.), European Research Council (AuxinER - ERC starting grant 639478 to J.K.-V.), the Austrian Science Fund (FWF) (grant number P26333 to M.K).

Materials and Methods

Plant material

The Wt background for all lines described is Col-0. Lines *mur2-1* (Vanzin et al., 2002), *axy8-1* (Günl et al., 2011), *mur3-3* (Kong et al., 2015) and *bgal10-1* (Sampedro et al., 2012) have been previously described. The *axy8-1* line was courtesy of Markus Pauly, *mur3-3* was courtesy of Malcom O´Neill and *bgal10-1* was courtesy of Ignacio Zarra. 35s::PILS5-GFP (*PILS5*^{OE}) was described in Barbez et al. 2012 (Barbez et al., 2012). *xth30-1* (Salk_045361) and *xth33-1* (Salk_072153) were obtained from Nottingham Arabidopsis Stock Centre. Primers used for genotyping are listed on STable3.

Growth Conditions

Seeds were sterilized overnight with chlorine gas, and afterwards plated in 0.8% agar, 0.5xMurashige and Skoog (MS), and 1% sucrose medium (MS+). For the majority of the experiments (unless stated otherwise), the plates containing the seeds were stratified for two days at 4^{o}C, and after, they were exposed to cool-white light (140µmol.m^{-2}.s^{-1}) for 8 hs at 21^{o} so as to induce germination, and later kept in the dark for five days at 21^{o}C.
For the auxin treatment experiments, the MS medium was supplemented with 800nM IAA or less than 0.1% DMSO. The seedlings were placed on this medium and grown as described above.

RNA extraction and RT-qPCR Analysis

We always used hypocotyl tissue for RNA extractions. For the Kynurenine treatments and the estradiol –induced assays, a 100 µm pore mesh (Mesh Nitex 03-100/44; Transalpina) was placed on top the MS+ medium, and then the seeds were placed on top of this mesh. The plates were then handled as described above for five days (Kyn treatments), or three days (estradiol treatments). At day 5 (or 3), the plates were uncovered under a green light, so as not to activate any light responses, and the mesh was transferred onto a new plate

containing either 30µM Kynurenine (He et al., 2011) or 10µM β-estradiol, and then kept in the dark overnight (Kyn) or for 3hs (estradiol), respectively. Tissue was harvested afterwards and total RNA was isolated using the InnuPREP Plant RNA Kit (Analytic Jena), following the manufacturer's instructions. After RNA extraction, samples were treated with InnuPREP DNase I (Analytic Jena). cDNA was synthesized from 1µg of RNA using the iSCRIPT cDNA synthesis Kit (Bio-Rad) following manufacturer's recommendations. We used Takyon qPCR Kit for SYBER assay (Eurogentec) and the RT-PCR was carried out in CFX96 Touch Real-Time PCR Detection System (Bio-Rad). ACT2 was used as housekeeping unless stated otherwise. For RNAseq validations, gene AT1G29670 was used as housekeeping, since it was a gene that was stable for all lines and treatments. This gene was selected from the RNAseq data. Primers for all tested genes are listed in STable3.

Cloning

Gateway cloning was used to construct estradiol inducible pMDC7_B(pUBQ):*GH3.6.* The *GH3.6* full-length genomic fragment was amplified by PCR from genomic DNA. Primers are listed in STable3. The PCR was performed using the high fidelity DNA polymerase "I proof" (Bio-Rad). The full genomic fragments were cloned into the pDONR221 (Invitrogen) vector using Invitrogen BP-clonase according to manufacturer's instructions. Coding sequences were transferred from the entry clones to gateway-compatible pMDC7_B(pUBQ) vector (Barbez et al., 2012) using the Invitrogen LR clonase according to manufacturer's instructions. Inducible *PILS5* was analogously cloned using the *PILS5* entry clone (Barbez et al., 2012). The resulting construct as well as an empty vector were transformed into Col-0 plants by floral dipping in *Agrobacterium tumefaciens* GV3101 strain liquid cultures.

Quantification of Hypocotyl Length and Gravity index

Seedlings were grown for five days in the dark on vertically orientated plates. After this, the plates were scanned with an Epson Perfection V700 scanner. Hypocotyl length was quantified using FIJI 2.0 software (Schindelin et al., 2012).
The Gravity index was calculated as the ratio between the total hypocotyl length and the distance between the apex and the base of the hypocotyl.

Gravi-stimulation assays and quantification

Seedlings were grown for four days and then turned 90^{o} and kept in this position for another 24hs. Afterwards, plates were scanned with an Epson Perfection V700 scanner. We measured the angle that was formed between the apex of the hypocotyl and the gravity vector, using the angle tool of the FIJI software.

Real time analysis of gravitropic response

Seedlings were grown for 4 days and then turned 90^{o} then placed in this new position in light-sealed box equipped with an infrared light source (880 nm LED) and a spectrum-

enhanced camera (EOS035 Canon Rebel T3i) (Béziat et al., 2017). The angles made between the hypocotyl apex and the gravity vector were measured every 30min with the angle tool of FIJI. Representative experiments are shown. Gravitropism kinetics was statistically analyzed using a non-linear regression fit to a one-phase association curve (Béziat et al., 2017).

Confocal Imaging and Quantification

Imaging was performed using a Leica TCS SP% confocal microscope, equipped with HyD detector. The fluorescence signal intensity (Mean Gray Value) was quantified using the LEICA LAS AF Lite software. In all cases, a ROI was defined, and the signal intensity was quantified within that region. The same ROI was kept for all analyzed images within said experiment. ROIs used are indicated in the respective figures.

RNA sequencing

Three-day old seedlings of pMDC7::GH3.6, pER8::YUC6 (Mashiguchi et al., 2011) and pMDC7 empty vector lines were grown and induced as already described above. After the induction time, hypocotyl tissue was harvested and total RNA was extracted using the RNaeasy Plant Mini Kit (Qiagen) following manufacturer's instructions. Prior to cDNA synthesis, RNA was treated with the RNase-Free DNase Set (Qiagen) with the manufacturer's recommendations.

The RNA libraries and the subsequent sequencing were performed by the Next Generation Sequencing Facility from the Vienna Biocenter (https://www.viennabiocenter.org/facilities/next-generation-sequencing/). The libraries were generated with the NEBNext Ultra II RNA Library Prep Kit for Illumina with poly(A) enrichment. The sequencing was performed on an Illumina HiSeq2500 with 250bp paired ended fragments.

Bioinformatics' Analysis of the RNAseq data

Accession numbers

Datasets and NCBI SRA accession numbers will be available shortly.

Data pre-processing

Ribosomal RNA reads were removed by mapping the raw reads against the ribosomal transcript sequences using bwa mem [0.7.16a-r1181, (Li, 2013)]. The paired end reads were extracted from the unmapped reads using bedtools bamToFastq [v2.29.0, (Quinlan and Hall, 2010)] and the Illumina TruSeq adapters were trimmed with cutadapt (Martin, 2011).

Differential expression analysis

To determine differential expression of the pER8::YUC6 and pMDC7::GH3.6 compared to the pMDC7 Empty vector we considered the transcript per million (TPM) values estimated with

Salmon [v0.9.1, (Patro et al., 2017)] for the AtRTD2-QUASI transcriptome annotation (Zhang et al., 2017), and used tximport (Soneson et al., 2015) to aggregate the transcript read counts per gene. Differentially expressed genes were obtained with edgeR using the exactTest (Robinson et al., 2010). Genes were considered differentially expressed for a false discovery rate < 0.05.

GO-term Analysis

GO-term analysis was performed using the PANTHER Overrepresentation Test (Released 2019.07.11). The enrichment was determined comparing the query list of differentially expressed genes with an *A.thaliana* database using a FISHER test with an FDR<0.05.

Atomic Force Measurements and Apparent Young's Modulus Calculations

The AFM data were collected and analyzed as described elsewhere with minor changes (Peaucelle et al., 2015) To examine extracellular matrix properties we suppress the turgor pressure by immersion of the seedlings in a hypertonic solution (0.55 M mannitol). Three day-old seedlings grown in darkness (in normal AM plate, with or without IAA) were placed in microscopy slides and immobilized using double-glued side tape. We focused on the anticlinal (perpendicular to the organ surface) cell walls and its extracellular matrix. To ensure proper indentations, especially on the regions in the bottom of the doom shape between two adjacent cells, we used cantilevers with long pyramidal tip (14-16 µm of pyramidal height, AppNano ACST-10), with a spring constant of 7.8 N/m. The instrument used was a JPK Nano-Wizard 4.0 and indentations were kept to <10% of cell height. Three scan-maps per sample were taken over an intermediate region of the hypocotyls, using a square area of 25 x 25 µm, with 16 x 16 measurements, resulting in 1792 force-indentation experiments per sample. The lateral deflection of the cantilever was monitored and in case of any abnormal increase the entire data set was not used for analysis. The apparent Young's modulus (E_A) for each force-indentation experiment was calculated using the approach curve (to avoid any adhesion interference) with the JPK Data Processing software (JPK Instruments AG, Germany). To calculate the average E_A for each anticlinal wall, the E_A was measured over the total length of the extracellular region using masks with Gwyddion 2.45 software (at least 20 points were taken in account). The pixels corresponding to the extracellular matrix were chosen based on the topography map. For topographical reconstructions, the height of each point was determined by the point-of-contact from the force-indentation curve. A total of 12-14 samples were analyzed. A standard t-test was applied to test for differences between genotypes.

Monosaccharide composition of Polysaccharides

The analysis was performed using four day-old dark grown hypocotyls on MS half strength supplemented with sucrose. Two grams of this tissue were used to prepare alcohol-insoluble material to be used in the later analysis. For this purpose, hypocotyls were washed twice in four volumes of absolute ethanol for 15 min, then rinsed twice in four volumes of

acetone at room temperature for 10min and left to dry under a fume hood overnight at room temperature. For determining the neutral monosaccharide composition, 10 mg of dried alcohol-insoluble material were hydrolyzed in 2.5 M trifluoroacetic acid for 1 h at 100^{o}C as described by (Harholt et al., 2006).

Xyloglucan Fingerprinting (OLIMP)

Using a green light, four-day old dark-grown seedlings were collected and stored in cold ethanol. Five hypocotyls were dissected for each biological repeat (n = 4), and later used for the analysis. After being left overnight at room temperature in ethanol, the ethanol was removed and the hypocotyls were dried at 37°C for 1 h. Afterwards, 20µl of 50mM acetate buffer, pH5.0, containing endoglucanase from *Trichoderma longibrachiatum* (Magzyme) were added and left overnight at 37°C. OLIMP was then carried out as reported by (Lerouxel et al., 2002) using Super DHB matrix (9:1 mixture of DHB and 2-hydroxy-5-methoxybenzoic acid; Fluka) instead of DHB.

Inmunostainings

Arabidopsis hypocotyl section of two days-old seedlings were fixed in 4% paraformaldehyde (PFA) in phosphate buffered saline (PBS) for 45 mins afterward washed 4 times with PBS buffer. Samples were dehydrated for 30 mins sequentially at 30%, 50%, 70%, 90% and 100% EtOH in PBS. LR white was added to samples dropwise to 10% and incubated at 4°C for 6hs. Afterwards, solution was exchanged with 30% LR white in PBS and incubated at 4°C overnight. Solution was exchange with 100% LR white subsequently for 3 times each with 12hs incubation and polymerized at 60°C for 36 hrs. Samples were sectioned at 2.5uM thickness using a Reichert Ultracut S Wild M3Z microtome mounted with a Diatome Histo Diamond Knife (8.0mm 45° angle). Sections were placed on glass slides. Inmunolabelling was performed on sections using CCRC-M1 primary antibody (Agrisera) (Puhlmann et al., 1994) with 1:100 dilution with PBS buffer. Secondary antibody anti Rat Cy5 (Jacksson Immunoresearch) was used with dilution of 1:200. Images were taken using Carl Zeiss LSM780 using 40X magnification (Zeiss C-Apochromat 40x/1.2W Corr M27). Cy5 was excited at 633 nM.

Data Analysis

All graphs and statistical analysis were made with the GraphPad Prism 5 software. All experiments were performed at least three times.

Figures

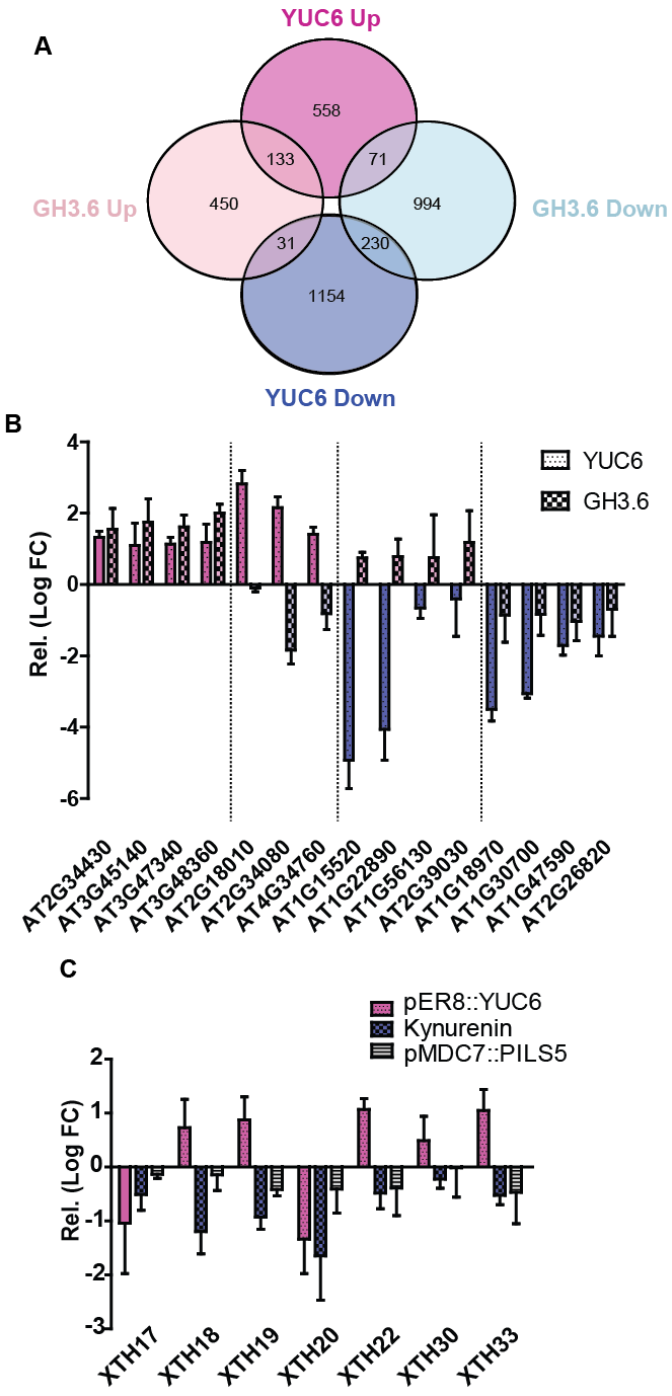

Fig.1. RNA sequencing of estradiol-inducible GH3.6 and YUC6 lines. Three-day old dark-grown hypocotyls were induced for three hours with 10μM β-Estradiol. **A)** Venn diagram depicting the number of genes that were differentially up-regulated or down-regulated when compared to the estradiol-treated empty vector control. **B)** Validation by RT-qPCR of a subset of the DEG belonging to the four categories in Fig.1A. The Log Fold Change (FC) values are relative to the treated empty vector control. Representative graph of three biological replicates. Data are mean ± SD (n = 3 and three technical repeats for each). **C)** RT-qPCR of selected members of the *Xyloglucan endotransglucosylase/hydrolase* (*XTH*) familyunder conditions of high auxin abundance (3hs estradiol induction of pER8::YUC6) and low auxin abundance (overnight treatment with 30μM Kynurenine and 3hs estradiol induction of pMDC7::PILS5). The Log Fold Change (FC) values are relative to the treated empty vector control for pER8::YUC6 and pMDC7::PILS5, and relative to the DMSO-treated control for the Kyn treatment. Representative graph of three biological replicates. Data are mean ± SD (n = 3 and three technical repeats for each).

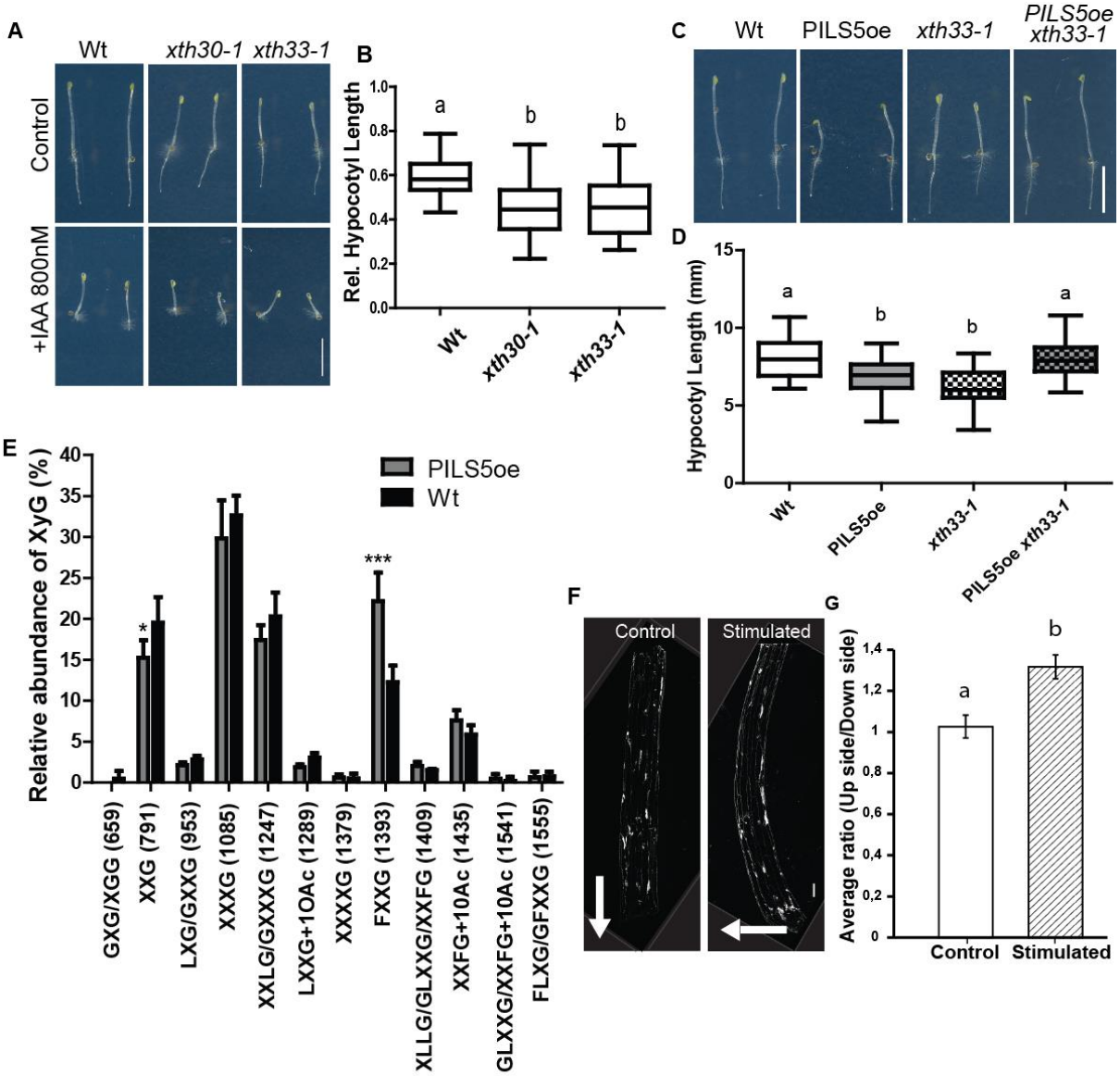

Fig.2. A-B) Auxin response of *xth30-1* and *xth33-1*. T-DNA-insertion mutants *xth30-1* and *xth33-1* were grown on 800nM IAA or DMSO (Control) for 5 days. **A)** Representative images. Scale bar = 5mm. **B)** Quantification of the hypocotyl length relative to the control treatment. Tukey box-plot. One-Way Anova with p-value<0.05 (n = 25 - 30). **C-D)** Genetic interaction between 35s::PILS5-GFP (PILS5^{oe}) and *xth33-1*. **C)** Representative images of 5-day old dark-grown hypocotyls. Scale bar = 5mm. **D)** Quantification of the hypocotyl length. Tukey box-plot. One-Way Anova followed by Tukey with p-value<0.05. (n = 15-25) **E)** Oligosaccharide mass profiling (OLIMP) on 5-day old dark-grown hypocotyls of 35s::PILS5-GFP. Data are mean ± SD (n = 3 and three technical repeats for each). T-test with p-value<0.05. **F-G)** Inmunolabeling with CCRC-M1 antibody of longitudinal sections of 5-day dark-grown hypocotyls after gravistimulation. CCRC-M1 detects fucosylated epitopes of XyG. Two-way Anova with p-value<0.05. **F)** Representative images of sections of Wt non-gravistimulated (Control) and 8hs gravistimulated (Stimulated). Scale bar = 100µm. **G)** Quantification of the ratio of the mean grey signal between the up side and the down side of the hypocotyl section. T-test with p-value<0.05 (n = 4 with 4 technical repeats each).

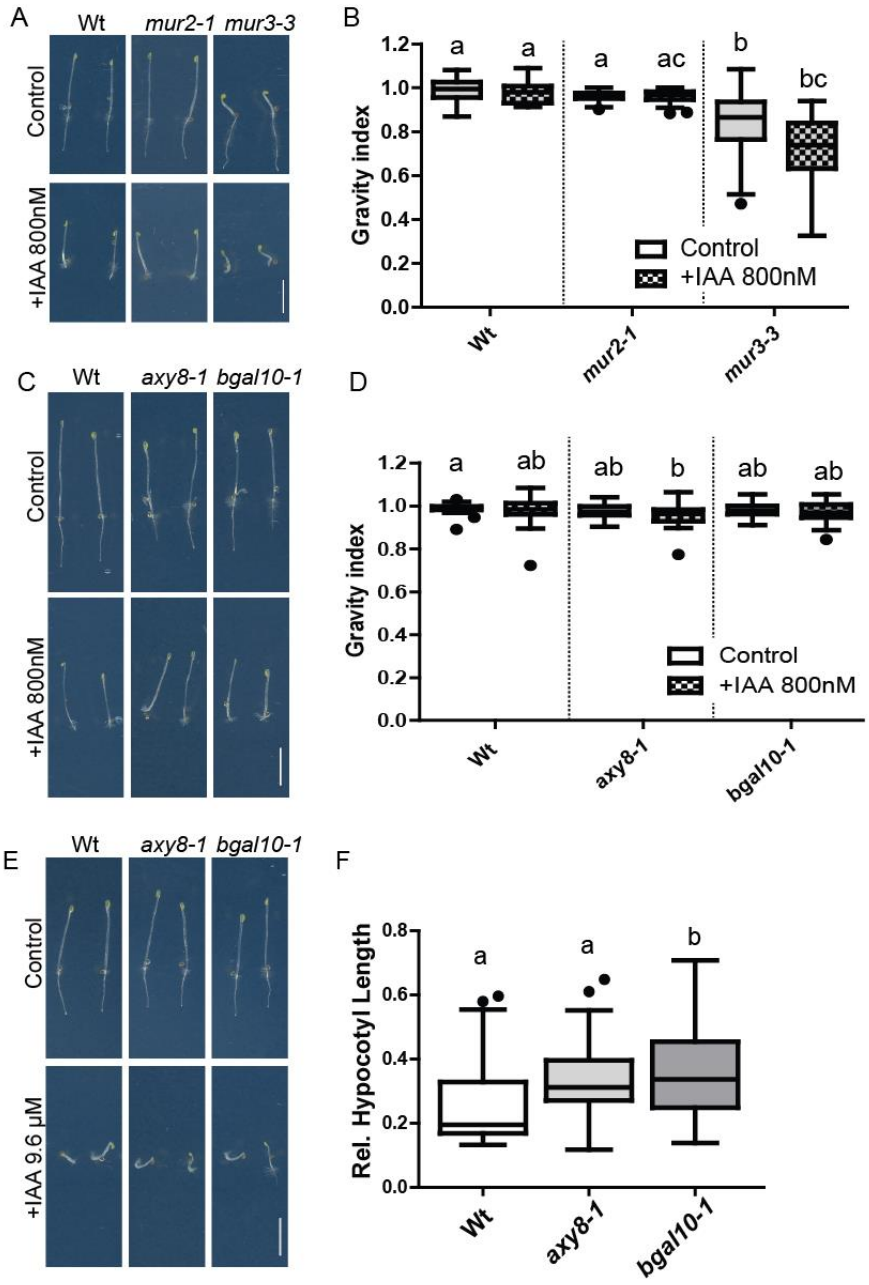

Fig.3. A-D) Galactosylation and Fucosylation of Xylogulcans. **A, C)** Mutants of galactosyltransferase *mur3-3* (A), fucosyltransferase *mur2-1*(A), galactosylhydrolase *bgal10-1* (C) and fucosylhydrolase *axy8-1* (C) were grown on 800nM IAA or DMSO (Control) for 5 days. **A, C)** Representative images of *mur2-1* (A), *mur3-3* (A), *axy8-1* (C) and *bgal10-1* (C). Scale bar = 5mm. **B, D)** Quantification of the Gravity index of *mur3-3* (B), *mur2-1* (B), *axy8-1* (D) and *bgal10-1* (D) after 800nM IAA or DMSO (Control) treatment. This index is the ratio between the total hypocotyl length and the distance between the apex and base of the hypocotyl. Tukey box-plot (biological repeats n = 25 - 35).Two-way Anova followed by Bonferroni with p-value<0.05 . **E-F)** *axy8-1* and *bgal10-1* grown on 9.6µM IAA or DMSO (Control). **E)** Representative images. Scale bar = 5mm. **F)** Quantification of the hypocotyl length relative to the DMSO-treated condition. Tukey box-plot (biological repeats n = 35 - 40). One-Way Anova with p-value<0.05.

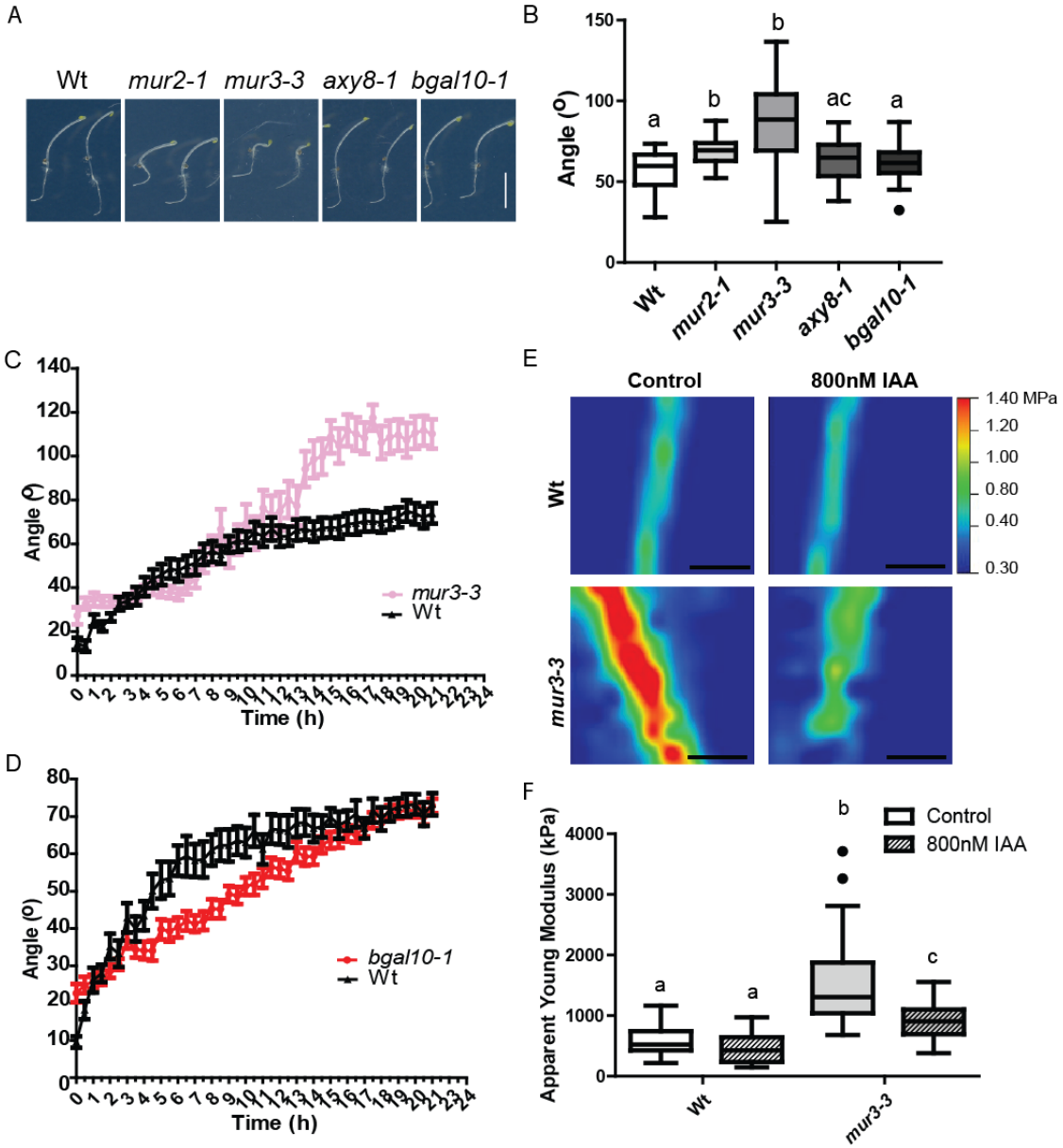

Fig.4. A-D) Response to gravistimulation of *mur2-1*, *mur3-3*, *axy8-1* and *bgal10-1*. **A-B)** Five-day old dark-grown hypocotyls were challenged with a 90^{o} angle change in growth orientation and the end point angle between the apex of the hypocotyl and gravity vector was measured 24hs later. **A)** Representative images of the angle after 24hs. **B)** Quantification of the end point angle. Tukey box-plot. One-Way Anova followed by Tukey. P-value<0.05. Scale bar = 5mm (n = 20-30). **C-D)** Growth kinetics of *mur3-3* and *bgal10-1*. Five-day old dark-grown hypocotyls were challenged with a 90^{o} angle change in growth orientation and placed in a dark-imaging box where their growth was recorded. The angle reached every 30 min was quantified. Non-linear fit to a one-phase association curve. K values for each curve were compared. P-value<0.05. Data are mean±SEM (n = 12 - 28). **E-F)** Atomic Force Microscopy (AFM) analysis of *mur3-3*. Dark-grown hypocotyls of *mur3-3* and Wt Col-0 were grown for three days on 800nM IAA or DMSO (Control). **E)** Representative images. Scale bar = 5µm. **F)** Quantification of Apparent Young Modulus in kPa. Tukey box-plot. One-Way Anova followed by tukey. P-value<0.05 (n =30-40).

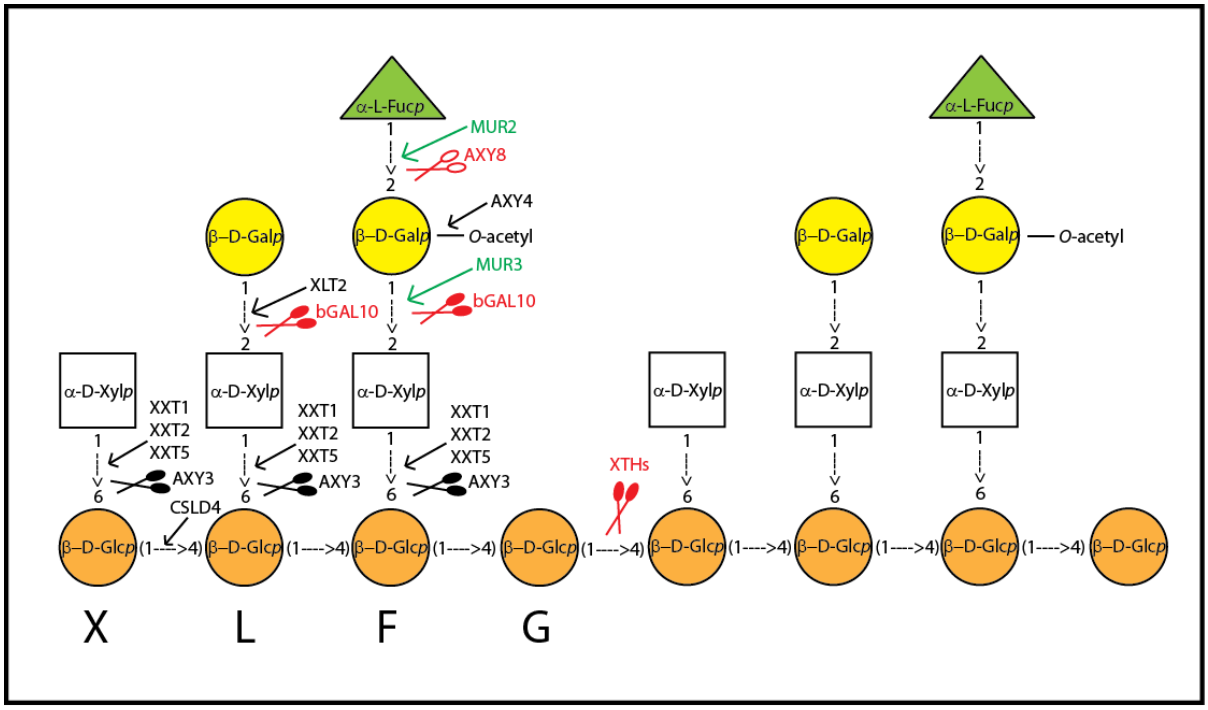

SFig.1. Schematic representation of the biosynthesis and "turnover" of Xyloglucans. The arrows and scissors mark the site of action of the different glycosyltransferases and glycosylhydrolases, respectively. In green, are the biosynthesis enzymes, and in red, the ones that are part of the turnover in the apoplast. In black are the enzymes not relevant for this study.

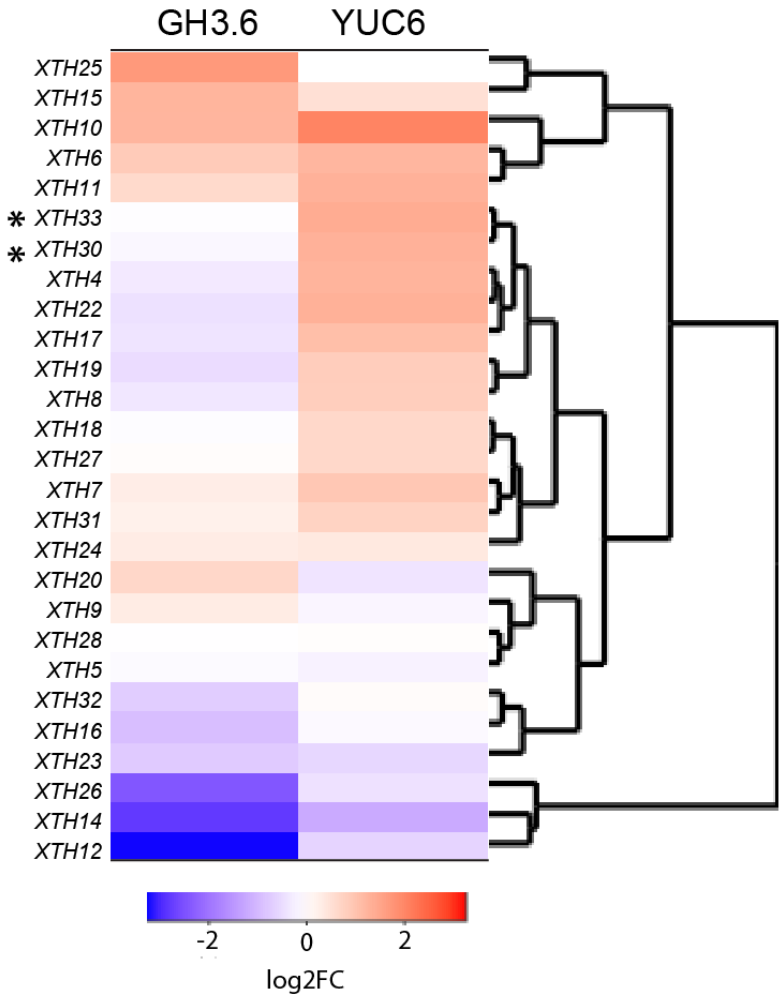

SFig2. Hierarchical cluster analysis of gene expression of XTH genes based on log FC ratio relative to the empty vector control. Blue represents lowest expression and red highest. Asteriks mark the two XTHs that were studied in more depth in this work.

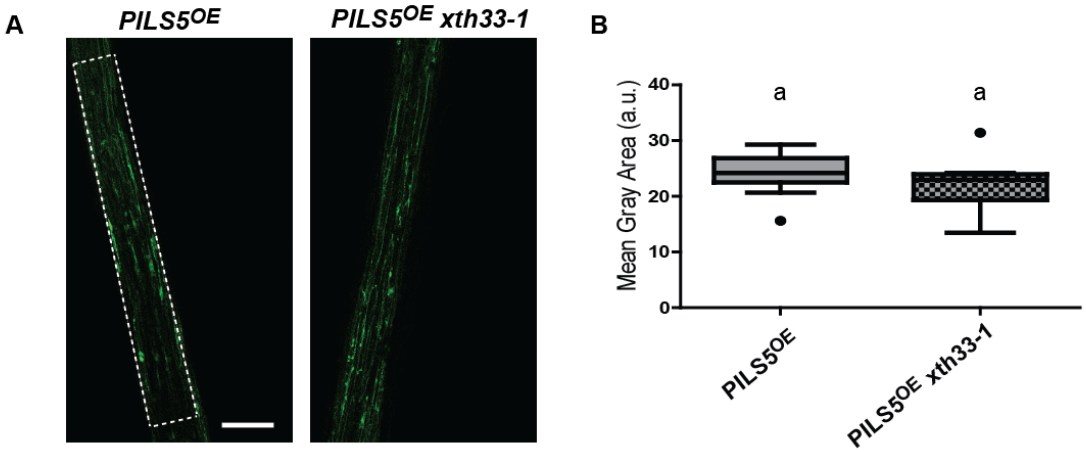

SFig.3. A-B) Confocal images of *PILS5^{OE} xth33-1* cross. Five-day old dark-grown seedlings were imaged. **A)** Representative images. White dashed-square marks the region that was quantified in each image. Scale bar 200µm. **B)** Quantification of signal intensity as Mean Gray Values in arbitrary units (a.u.). Tukey box-plot. T-test p-value<0.05 (n = 10).

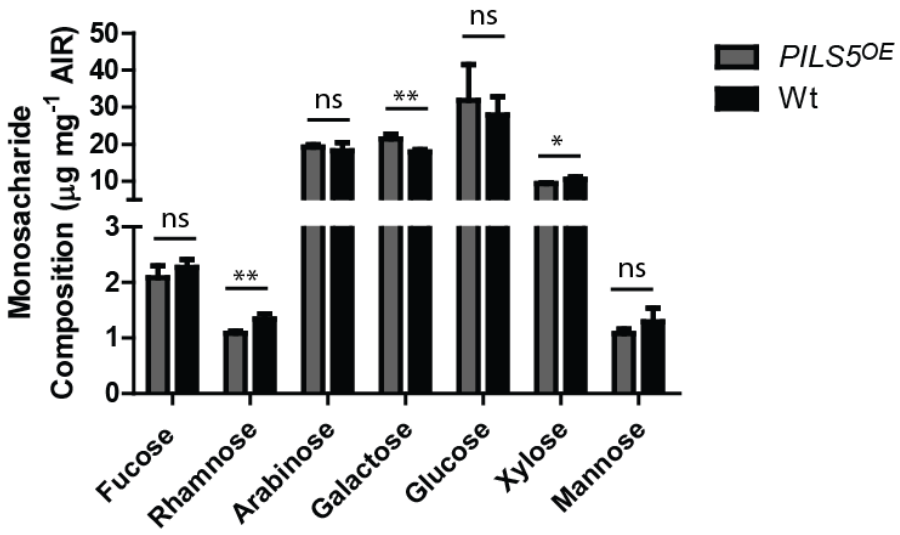

SFig.4. Monosaccharide composition of wall preparations from etiolated seedlings.

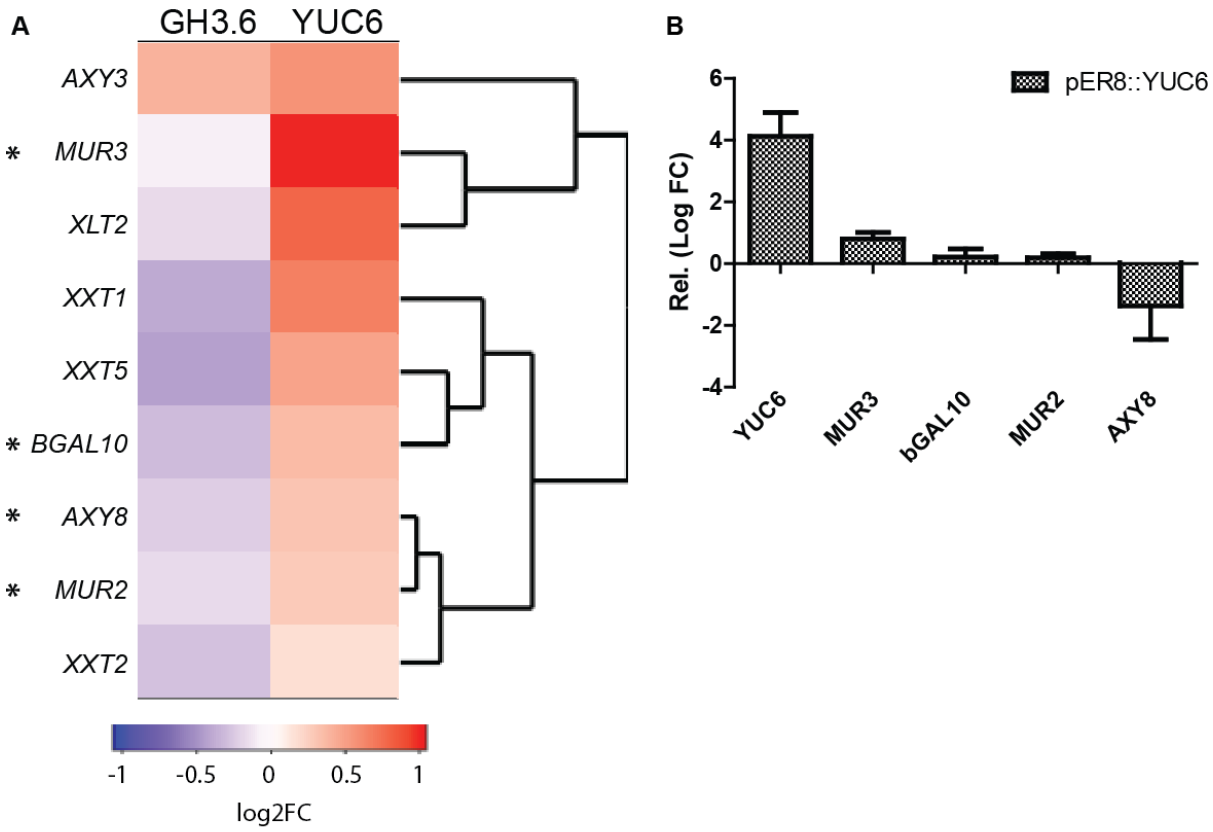

SFig5. A) Hierarchical cluster analysis of gene expression of XyG biosynthesis genes based on log FC ratio relative to the empty vector control. Blue represents lowest expression and red highest. Asteriks mark the genes studied in more depth within this work. **B)** RT-qPCR of XyG genes *MUR3*, *bGAL10*, *MUR2* and *AXY8* in the estradiol-inducible line pER8::YUC6. Three-day old dark-grown hypocotyls were induced for 3hs with 10µM β-Estradiol. Induction levels of the *YUC6* gene were evaluated. The Log Fold Change (FC) values are relative to the treated empty vector control.

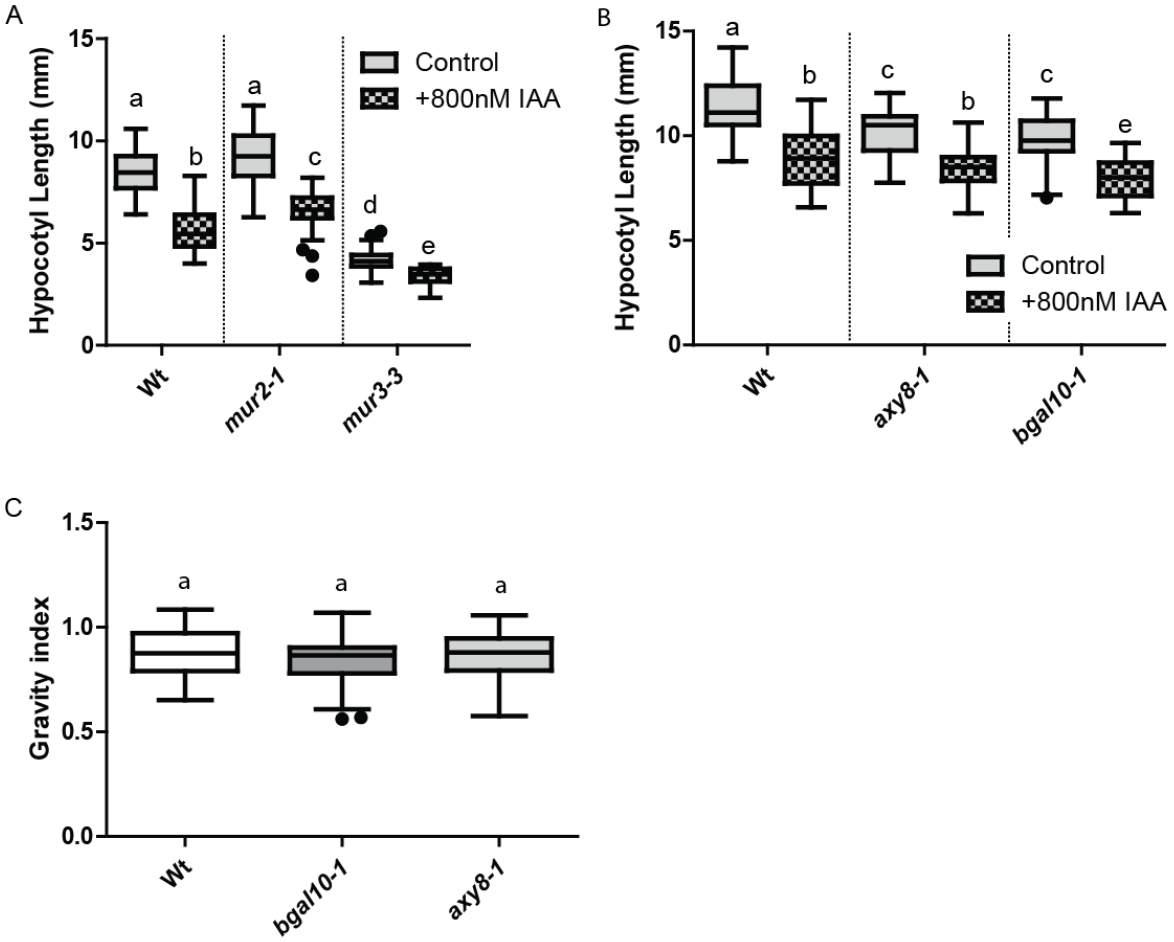

SFig.6. A-B) Auxin response of *mur2-1*, *mur3-3, axy8-1* and *bgal10-1*. All four T-DNA-insertion mutants were grown on 800nM IAA or DMSO (Control) for five days, and then the hypocotyl length was quantified for the treated and control condition. **A)** Quantification for *mur2-1* and *mur3-3*. Tukey box-plot (n = 25 - 35). One-Way Anova followed by Tukey. P-value<0.05. **B)** Quantification for *axy8-1* and *bgal10-1*. Tukey box-plot (n = 25 - 35). One-Way Anova followed by Tukey with p-value<0.05. **C)** Quantification of the Gravity index of *axy8-1* and *bgal10-1* after 9.6 µM IAA or DMSO (Control) treatment. This index is the ratio between the total hypocotyl length and the distance between the apex and base of the hypocotyl. Tukey box-plot (n = 35 - 40). Two-way Anova followed by Bonferroni with p-value<0.05.

Supplemental Tables' Legends

STable1. List of differentially expressed genes from the RNAseq. **SFile1**. Differential expressed genes of pER8::YUC6 vs pMDC7 Empty vector. **SFile2.** Differential expressed genes of pMDC7::GH3.6 vs pMDC7 Empty vector. **SFile3.**Differentially expressed genes shared between pER8::YUC6 and pMDC7::GH3.6 in the up-regulated category. **SFile4.** Differentially expressed genes shared between pER8::YUC6 and pMDC7::GH3.6 that are up-regulated in YUC6 and down-regulated in GH3.6. **SFile5.** Differentially expressed genes shared between pER8::YUC6 and pMDC7::GH3.6 that are down-regulated in YUC6 and up-

regulated in GH3.6. **SFile6.** Differentially expressed genes shared between pER8::YUC6 and pMDC7::GH3.6 in the down-regulated category.

STable2. GO-term analysis of the four categories determined from the RNAseq data for the differentially expressed genes: (I) up- or (II) down-regulation in both, (III) up- and down- or (IV) down- and up- in YUC6 and GH3.6. The analysis was performed using the PANTHER Overrepresentation Test.

STable3. List of primers used in this study.

References

Barbez, E., Dünser, K., Gaidora, A., Lendl, T., and Busch, W. (2017). Auxin steers root cell expansion via apoplastic pH regulation in Arabidopsis thaliana. Proceedings of the National Academy of Sciences 114:E4884-E4893.

Barbez, E., Kubeš, M., Rolčík, J., Béziat, C., Pěnčík, A., Wang, B., Rosquete, M.R., Zhu, J., Dobrev, P.I., and Lee, Y. (2012). A novel putative auxin carrier family regulates intracellular auxin homeostasis in plants. Nature 485:119-122.

Béziat, C., Barbez, E., Feraru, M.I., Lucyshyn, D., and Kleine-Vehn, J. (2017). Light triggers PILS-dependent reduction in nuclear auxin signalling for growth transition. Nature plants 3:17105.

Calderón Villalobos, L.I.A., Lee, S., De Oliveira, C., Ivetac, A., Brandt, W., Armitage, L., Sheard, L.B., Tan, X., Parry, G., Mao, H., et al. (2012). A combinatorial TIR1/AFB–Aux/IAA co-receptor system for differential sensing of auxin. Nature Chemical Biology 8:477-485.

Catalá, C., Rose, J.K., and Bennett, A.B. (1997). Auxin regulation and spatial localization of an endo-1, 4-β-d-glucanase and a xyloglucan endotransglycosylase in expanding tomato hypocotyls. The Plant Journal 12:417-426.

Catalá, C., Rose, J.K., York, W.S., Albersheim, P., Darvill, A.G., and Bennett, A.B. (2001). Characterization of a tomato xyloglucan endotransglycosylase gene that is down-regulated by auxin in etiolated hypocotyls. Plant Physiology 127:1180-1192.

Cavalier, D.M., Lerouxel, O., Neumetzler, L., Yamauchi, K., Reinecke, A., Freshour, G., Zabotina, O.A., Hahn, M.G., Burgert, I., and Pauly, M. (2008). Disrupting two Arabidopsis thaliana xylosyltransferase genes results in plants deficient in xyloglucan, a major primary cell wall component. The Plant Cell 20:1519-1537.

Cheng, Y., Dai, X., and Zhao, Y. (2006). Auxin biosynthesis by the YUCCA flavin monooxygenases controls the formation of floral organs and vascular tissues in Arabidopsis. Genes & development 20:1790-1799.

Cosgrove, D.J. (2005). Growth of the plant cell wall. Nat Rev Mol Cell Biol 6:850-861.

Cosgrove, D.J. (2014). Re-constructing our models of cellulose and primary cell wall assembly. Current opinion in plant biology 22:122-131.

Dünser, K., and Kleine-Vehn, J. (2015). Differential growth regulation in plants—the acid growth balloon theory. Current opinion in plant biology 28:55-59.

Farkas, V., Sulova, Z., Stratilova, E., Hanna, R., and Maclachlan, G. (1992). Cleavage of xyloglucan by nasturtium seed xyloglucanase and transglycosylation to xyloglucan subunit oligosaccharides. Archives of biochemistry and biophysics 298:365-370.

Fendrych, M., Akhmanova, M., Merrin, J., Glanc, M., Hagihara, S., Takahashi, K., Uchida, N., Torii, K.U., and Friml, J. (2018). Rapid and reversible root growth inhibition by TIR1 auxin signalling. Nature plants 4:453.

Fendrych, M., Leung, J., and Friml, J. (2016). TIR1/AFB-Aux/IAA auxin perception mediates rapid cell wall acidification and growth of Arabidopsis hypocotyls. Elife 5.

Feraru, E., Feraru, M.I., Barbez, E., Waidmann, S., Sun, L., Gaidora, A., and Kleine-Vehn, J. (2019). PILS6 is a temperature-sensitive regulator of nuclear auxin input and organ growth in Arabidopsis thaliana. Proceedings of the National Academy of Sciences 116:3893-3898.

Franková, L., and Fry, S.C. (2013). Biochemistry and physiological roles of enzymes that 'cut and paste'plant cell-wall polysaccharides. Journal of Experimental Botany 64:3519-3550.

Fry, S., Smith, R., Renwick, K., Martin, D., Hodge, S., and Matthews, K. (1992a). Xyloglucan endotransglycosylase, a new wall-loosening enzyme activity from plants. Biochemical Journal 282:821-828.

Fry, S.C. (1997). Novel 'dot-blot' assays for glycosyltransferases and glycosylhydrolases: optimization for xyloglucan endotransglycosylase (XET) activity. The Plant Journal 11:1141-1150.

Fry, S.C., Smith, R.C., Renwick, K.F., Martin, D.J., Hodge, S.K., and Matthews, K.J. (1992b). Xyloglucan endotransglycosylase, a new wall-loosening enzyme activity from plants. Biochemical Journal 282:821-828.

Günl, M., Neumetzler, L., Kraemer, F., de Souza, A., Schultink, A., Pena, M., York, W.S., and Pauly, M. (2011). AXY8 encodes an α-fucosidase, underscoring the importance of apoplastic metabolism on the fine structure of Arabidopsis cell wall polysaccharides. The Plant Cell 23:4025-4040.

Harholt, J., Jensen, J.K., Sørensen, S.O., Orfila, C., Pauly, M., and Scheller, H.V. (2006). ARABINAN DEFICIENT 1 is a putative arabinosyltransferase involved in biosynthesis of pectic arabinan in Arabidopsis. Plant physiology 140:49-58.

He, W., Brumos, J., Li, H., Ji, Y., Ke, M., Gong, X., Zeng, Q., Li, W., Zhang, X., and An, F. (2011). A small-molecule screen identifies L-kynurenine as a competitive inhibitor of TAA1/TAR activity in ethylene-directed auxin biosynthesis and root growth in Arabidopsis. The Plant Cell 23:3944-3960.

Jensen, J.K., Schultink, A., Keegstra, K., Wilkerson, C.G., and Pauly, M. (2012). RNA-Seq analysis of developing nasturtium seeds (Tropaeolum majus): identification and characterization of an additional galactosyltransferase involved in xyloglucan biosynthesis. Molecular plant 5:984-992.

Kong, Y., Peña, M.J., Renna, L., Avci, U., Pattathil, S., Tuomivaara, S.T., Li, X., Reiter, W.-D., Brandizzi, F., and Hahn, M.G. (2015). Galactose-depleted xyloglucan is dysfunctional and leads to dwarfism in Arabidopsis. Plant physiology 167:1296-1306.

Lavy, M., and Estelle, M. (2016). Mechanisms of auxin signaling. Development 143:3226-3229.

Lerouxel, O., Choo, T.S., Séveno, M., Usadel, B., Faye, L.c., Lerouge, P., and Pauly, M. (2002). Rapid structural phenotyping of plant cell wall mutants by enzymatic oligosaccharide fingerprinting. Plant Physiology 130:1754-1763.

Li, H. (2013). Aligning sequence reads, clone sequences and assembly contigs with BWA-MEM. arXiv preprint arXiv:1303.3997.

Lorences, E.P., and Fry, S.C. (1993). Xyloglucan oligosaccharides with at least two α-d-xylose residues act as acceptor substrates for xyloglucan endotransglycosylase and promote the depolymerisation of xyloglucan. Physiologia Plantarum 88:105-112.

Madson, M., Dunand, C., Li, X., Verma, R., Vanzin, G.F., Caplan, J., Shoue, D.A., Carpita, N.C., and Reiter, W.-D. (2003). The MUR3 gene of Arabidopsis encodes a xyloglucan galactosyltransferase that is evolutionarily related to animal exostosins. The Plant Cell Online 15:1662-1670.

Majda, M., and Robert, S. (2018). The role of auxin in cell wall expansion. International journal of molecular sciences 19:951.

Martin, M. (2011). Cutadapt removes adapter sequences from high-throughput sequencing reads. EMBnet. journal 17:10-12.

Mashiguchi, K., Tanaka, K., Sakai, T., Sugawara, S., Kawaide, H., Natsume, M., Hanada, A., Yaeno, T., Shirasu, K., and Yao, H. (2011). The main auxin biosynthesis pathway in Arabidopsis. Proceedings of the National Academy of Sciences 108:18512-18517.

McDougall, G.J., and Fry, S.C. (1989). Structure-activity relationships for xyloglucan oligosaccharides with antiauxin activity. Plant Physiology 89:883-887.

Nishitani, K., and Tominaga, R. (1992). Endo-xyloglucan transferase, a novel class of glycosyltransferase that catalyzes transfer of a segment of xyloglucan molecule to another xyloglucan molecule. Journal of Biological Chemistry 267:21058-21064.

Osato, Y., Yokoyama, R., and Nishitani, K. (2006). A principal role for AtXTH18 in Arabidopsis thaliana root growth: a functional analysis using RNAi plants. Journal of plant research 119:153-162.

Pacheco-Villalobos, D., Díaz-Moreno, S.M., van der Schuren, A., Tamaki, T., Kang, Y.H., Gujas, B., Novak, O., Jaspert, N., Li, Z., and Wolf, S. (2016). The effects of high steady state auxin levels on root cell elongation in Brachypodium. The Plant Cell 28:1009-1024.

Patro, R., Duggal, G., Love, M.I., Irizarry, R.A., and Kingsford, C. (2017). Salmon provides fast and bias-aware quantification of transcript expression. Nature methods 14:417.

Peaucelle, A., Wightman, R., and Höfte, H. (2015). The control of growth symmetry breaking in the Arabidopsis hypocotyl. Current Biology 25:1746-1752.

Peña, M.J., Ryden, P., Madson, M., Smith, A.C., and Carpita, N.C. (2004). The galactose residues of xyloglucan are essential to maintain mechanical strength of the primary cell walls in Arabidopsis during growth. Plant Physiology 134:443-451.

Puhlmann, J., Bucheli, E., Swain, M.J., Dunning, N., Albersheim, P., Darvill, A.G., and Hahn, M.G. (1994). Generation of Monoclonal Antibodies against Plant Cell-Wall Polysaccharides (I. Characterization of a Monoclonal Antibody to a Terminal [alpha]-(1-> 2)-Linked Fucosyl-Containing Epitope. Plant Physiology 104:699-710.

Quinlan, A.R., and Hall, I.M. (2010). BEDTools: a flexible suite of utilities for comparing genomic features. Bioinformatics 26:841-842.

Rakusová, H., Gallego-Bartolomé, J., Vanstraelen, M., Robert, H.S., Alabadí, D., Blázquez, M.A., Benková, E., and Friml, J. (2011). Polarization of PIN3-dependent auxin transport for hypocotyl gravitropic response in Arabidopsis thaliana. The Plant Journal 67:817-826.

Reiter, W.D., Chapple, C., and Somerville, C.R. (1997). Mutants of Arabidopsis thaliana with altered cell wall polysaccharide composition. The Plant Journal 12:335-345.

Robinson, M.D., McCarthy, D.J., and Smyth, G.K. (2010). edgeR: a Bioconductor package for differential expression analysis of digital gene expression data. Bioinformatics 26:139-140.

Rosquete, M.R., Barbez, E., and Kleine-Vehn, J. (2012). Cellular auxin homeostasis: gatekeeping is housekeeping. Molecular plant 5:772-786.

Sampedro, J., Gianzo, C., Iglesias, N., Guitián, E., Revilla, G., and Zarra, I. (2012). AtBGAL10 is the main xyloglucan β-galactosidase in Arabidopsis, and its absence results in unusual xyloglucan subunits and growth defects. Plant physiology 158:1146-1157.

Sánchez, M., Gianzo, C., Sampedro, J., Revilla, G., and Zarra, I. (2003). Changes in α-xylosidase during intact and auxin-induced growth of pine hypocotyls. Plant and cell physiology 44:132-138.

Sauer, M., and Kleine-Vehn, J. (2019). PIN-FORMED and PIN-LIKES auxin transport facilitators. Development 146:dev168088.

Sauer, M., Robert, S., and Kleine-Vehn, J. (2013). Auxin: simply complicated. Journal of Experimental Botany 64:2565-2577.

Schindelin, J., Arganda-Carreras, I., Frise, E., Kaynig, V., Longair, M., Pietzsch, T., Preibisch, S., Rueden, C., Saalfeld, S., and Schmid, B. (2012). Fiji: an open-source platform for biological-image analysis. Nature methods 9:676-682.

Schultink, A., Liu, L., Zhu, L., and Pauly, M. (2014). Structural diversity and function of xyloglucan sidechain substituents. Plants 3:526-542.

Soneson, C., Love, M.I., and Robinson, M.D. (2015). Differential analyses for RNA-seq: transcript-level estimates improve gene-level inferences. F1000Research 4.

Staswick, P.E., Serban, B., Rowe, M., Tiryaki, I., Maldonado, M.T., Maldonado, M.C., and Suza, W. (2005). Characterization of an Arabidopsis enzyme family that conjugates amino acids to indole-3-acetic acid. The Plant Cell 17:616-627.

Talbott, L.D., and Ray, P.M. (1992). Changes in Molecular Size of Previously Deposited and Newly Synthesized Pea Cell Wall Matrix Polysaccharides. Effects of Auxin and Turgor 98:369-379.

Vanzin, G.F., Madson, M., Carpita, N.C., Raikhel, N.V., Keegstra, K., and Reiter, W.-D. (2002). The mur2 mutant of Arabidopsis thaliana lacks fucosylated xyloglucan because of a lesion in fucosyltransferase AtFUT1. Proceedings of the National Academy of Sciences 99:3340-3345.

Vissenberg, K., Martinez-Vilchez, I.M., Verbelen, J.-P., Miller, J.G., and Fry, S.C. (2000). In vivo colocalization of xyloglucan endotransglycosylase activity and its donor substrate in the elongation zone of Arabidopsis roots. The Plant Cell 12:1229-1237.

Vissenberg, K., Oyama, M., Osato, Y., Yokoyama, R., Verbelen, J.-P., and Nishitani, K. (2005). Differential expression of AtXTH17, AtXTH18, AtXTH19 and AtXTH20 genes in Arabidopsis roots. Physiological roles in specification in cell wall construction. Plant and Cell Physiology 46:192-200.

Xu, W., Purugganan, M.M., Polisensky, D.H., Antosiewicz, D.M., Fry, S.C., and Braam, J. (1995). Arabidopsis TCH4, regulated by hormones and the environment, encodes a xyloglucan endotransglycosylase. The Plant Cell 7:1555-1567.

York, W.S., Darvill, A.G., and Albersheim, P. (1984). Inhibition of 2, 4-dichlorophenoxyacetic acid-stimulated elongation of pea stem segments by a xyloglucan oligosaccharide. Plant Physiology 75:295-297.

Zhang, R., Calixto, C.P., Marquez, Y., Venhuizen, P., Tzioutziou, N.A., Guo, W., Spensley, M., Entizne, J.C., Lewandowska, D., and Ten Have, S. (2017). A high quality Arabidopsis transcriptome for accurate transcript-level analysis of alternative splicing. Nucleic acids research 45:5061-5073.

Zhang, T., Maruhnich, S.A., and Folta, K.M. (2011). Green light induces shade avoidance symptoms. Plant physiology 157:1528-1536.

Zhao, F., Chen, W.-Q., Sechet, J., Martin, M., Bovio, S., Lionnet, C., Long, Y., Battu, V., Mouille, G., and Monéger, F. (2019). Xyloglucans and microtubules synergistically maintain meristem geometry and phyllotaxis. Plant physiology:pp. 00608.02019.

STable 3. List of Primers used in this work

I. RT-qPCR

Name	Sequence	From
ACT2 F	TCGGTGGTTCCATTCTTGCT	(Zhang et al., 2011)
ACT2 R	GCTTTTTAAGCCTTTGATCTTGAGAG	(Zhang et al., 2011)
AXY8 F	TGATCTTGTGGATCCGTTGA	(Günl et al., 2011)
AXY8 R	GTGCCGGAGCAAATATAGA	(Günl et al., 2011)
bGAL10	GTCTACGGCGATACTGGTGG	
bGAL10	AGGGACGCTTCTGGGATAGT	
GH3.6 F	TCACCACCTATGCTGGGCTTTAC	
GH3.6 R	TGAAACCAGCCACGCTTAGGAC	
MUR3 F	ATTTCCTTGTGGCGGGTAGG	
MUR3 R	CTTGGCAGCCGGTAAGAAGA	
PILS5 F	TCAGACGGTTACACTTGAAGACA	
PILS5 R	GAAATGTAAGTCCCATGTTCACC	
XTH17 F	ATACTCCTGTGAGAACAAAATGAAG	
XTH17 R	CCCGCATAGACATGCACAGA	
XTH18 F	GTTTCCTCGAGGTGTTCCTGT	
XTH18 R	TCTTACACAAACACCGCATACAT	
XTH19 F	GAGGTGTTCCTCCAGAGTGC	
XTH19 R	AAAAGATCTTACACAAACACGCA	
XTH20 F	TTTTGCGGTAGAAGGTTCGC	
XTH20 R	AAGCTACCAGCGTAGACACG	
XTH22 F	GAACGCTGATGATTGGGCAA	
XTH22 R	AGCCAGTAGTAGTCCCCTGT	
XTH30 F	TCTCAATCTCAATCTCAGGCC	
XTH30 R	TCTGCTCCCATTGCATCGTT	
XTH33 F	GAACAGCCACTTAACTCCACG	
XTH33 R	CAGTGCAAGACTCAAGCTTCC	
YUC6 F	GCTCAGCCTTCTCTCGTTGT	
YUC6 R	CGAGGATGAACCGGGAAACA	
RNAseq Validation		
AT2G34430 F	TTCGCTACCAACTTCGTCCC	
AT2G34430 R	GCAACAAACCGGATACACACA	
AT3G45140 F	TCTCCAGTTTGATGCCCCAG	
AT3G45140 R	CATAAACGGCCGGGTCTAGT	
AT3G47340 F	GTTCCGATGATTCTCAGGCCA	
AT3G47340 R	TCAGGTCCTCTGTGCCTCAA	
AT3G48360 F	GCAAGCGGATGCTTCAACTC	
AT3G48360 R	GCAGACACAACCCTTGTCAC	
AT2G18010 F	TTTCCGGTTTACGTGGGACC	
AT2G18010 R	GAACTCGGAGTGATGGAGCC	
AT2G34080 F	CAAGTACCAAGGCCAATGCG	
AT2G34080 R	GGCGATCTTAGCCACACCTT	
AT4G34760 F	AGAGATGCTCGAGCTTAGGGA	
AT4G34760 R	TTGGTACGTCAAGCGGAAGG	
AT1G15520 F	TGACGCCTAACCACCACATC	
AT1G15520 R	TGGTACTTACGGGACGAGGG	
AT1G22890 F	ACAAGTTGGACTAGGCGAGG	
AT1G22890 R	AAATTGGAGGGGCCATGGAA	
AT1G56130 F	TTGACCGTTGTGATTGATTGTG	

Continuation I.RT-qPCR

AT1G56130 R	GATCTTCCAAGCCGCGAAAA
AT2G39030 F	GAGTCTGGTCTTGCCTCCAC
AT2G39030R	CCCCCTTTCTTGAGACGCAT
AT1G18970 F	GCAAATCAGCCGTTTCTGCT
AT1G18970 R	TCACTTGGCCAACGTTCCAT
AT1G30700 F	CCTCAAACTCCGACCCCAAA
AT1G30700 R	ACGGAGGAGTAGGAGCCATT
AT1G47590 F	CTACAGGTGTCGCGGAGAAG
AT1G47590 R	TAGGGCTTGTGGGTCTTGTG
AT2G26820 F	ACCAGGCAAAAGGCGTTACC
AT2G26820 R	TTACTTATGTCGTCTCCGGGC
AT1G29670 F	TCATCAGTCGCTACAGCACC
AT1G29670 R	TTGCTGAGTTGATGCGGTCT

II. Genotyping

Name	**Sequence**	**From**
mur3-3 F	TGCAAACGAAATTAAACATAGGC	(Kong et al., 2015)
mur3-3 R	GAAGAAGAAACTGATTGGGGC	(Kong et al., 2015)
xth30-1 F	TCTCAATCTCAATCTCAGGCC	
xth30-1 R	CGATAAGGGGTCAGCTTTTTC	
xth33-1 F	GAACAGCCACTTAACTCCACG	
xth33-1 R	CAGTGCAAGACTCAAGCTTCC	

III. Cloning

Name	**Sequence**
GH3.6 F for cloning	GGGGACAAGTTTGTACAAAAAAGCAGGCTCGATGCCTGAGGCACCAAAGAT
GH3.6 R for cloning	GGGGACCACTTTGTACAAGAAAGCTGGGTCTTAGTTACTCCCCCATTGCT